NeuroImage 57 (2011) 1447–1457

Contents lists available at ScienceDirect

NeuroImage

journal homepage: www.elsevier.com/locate/ynimg

A combination of atlas-based and voxel-wise approaches to analyze metabolic changes in autoradiographic data from Alzheimer's mice

J. Lebenberg [a], A.-S. Hérard [a], A. Dubois [b], M. Dhenain [a], P. Hantraye [a], T. Delzescaux [a,*]

[a] CEA-DSV-I2BM-MIRCen, CNRS URA2210, F-92265 Fontenay aux Roses Cedex, France
[b] CEA-DSV-I2BM-SHFJ, INSERM U803, F-91401 Orsay Cedex, France

ARTICLE INFO

Article history:
Received 21 January 2011
Revised 1 April 2011
Accepted 26 April 2011
Available online 4 May 2011

Keywords:
Biological image processing
Voxel-wise analysis
Region-of-interest analysis
Mouse brain atlas
Autoradiography

ABSTRACT

Murine models are commonly used in neuroscience research to improve our knowledge of disease processes and to test drug effects. To accurately study brain glucose metabolism in these animals, *ex vivo* autoradiography remains the gold standard. The analysis of 3D-reconstructed autoradiographic volumes using a voxel-wise approach allows clusters of voxels representing metabolic differences between groups to be revealed. However, the spatial localization of these clusters requires careful visual identification by a neuroanatomist, a time-consuming task that is often subject to misinterpretation. Moreover, the large number of voxels to be computed in autoradiographic rodent images leads to many false positives. Here, we proposed an original automated indexation of the results of a voxel-wise approach using an MRI-based 3D digital atlas, followed by the restriction of the statistical analysis using atlas-based segmentation, thus taking advantage of the specific and complementary strengths of these two approaches. In a preliminary study of transgenic Alzheimer's mice (APP/PS1), and control littermates (PS1), we were able to achieve prompt and direct anatomical indexation of metabolic changes detected between the two groups, revealing both hypo- and hypermetabolism in the brain of APP/PS1 mice. Furthermore, statistical results were refined using atlas-based segmentation: most interesting results were obtained for the hippocampus. We thus confirmed and extended our previous results by identifying the brain structures affected in this pathological model and demonstrating modified glucose uptake in structures like the olfactory bulb. Our combined approach thus paves the way for a complete and accurate examination of functional data from cerebral structures involved in models of neurodegenerative diseases.

Introduction

Murine models are commonly used to improve our understanding of the pathophysiology of neurodegenerative disorders such as Alzheimer's disease (AD) and to determine the effects of drugs. Functional alterations that occur early in the course of these diseases can be detected by brain imaging techniques. The use of *in vivo* imaging methods such as Positron Emission Tomography (PET) in the rodent brain poses a challenge because of the limited resolution of scans ($\simeq 500\ \mu m$) as compared to the size of the brain ($\simeq 0.5\ cm^3$) and because of the short acquisition time imposed by studies in live animals. To accurately study rodent brain function at a microscopic scale ($\simeq 20\ \mu m$), *ex vivo* [^{14}C]-2-deoxyglucose (2-DG) autoradiography thus remains the gold standard technique (Valla et al., 2006). This imaging method relies on the injection of a radioactive analog of glucose into the animal and its *post mortem* 2D localization in tissue sections. The standard method of analysis is to manually outline regions of interest (ROI) on images of these sections (Sadowski et al., 2004; Valla et al., 2006) with the help of a 2D atlas (Swanson, 1998; Paxinos and Franklin, 2001) or by directly superimposing digital sections from such atlases onto images from functional studies (Morrow et al., 1998; Paulson et al., 2007). However, this technique has several drawbacks.

The first major drawback of this technique is that the data yielded by such tissue sections is limited to two dimensions: the 3D spatial coherence of the structure is generally lost, and analysis is restricted to a limited number of sections. Moreover, the preparation of sections is a tedious process and the sections presented in the atlas do not occur exactly at the same level and are not equidistant throughout the organ. This adds to the difficulty in identifying the structures involved and their location. A considerable proportion of the information contained in these images thus remains unexploited. To overcome these limitations and thus create new possibilities for the analysis of functional data, several methods have been developed for the reconstruction of spatially coherent autoradiographic volumes from serial sections (Hess et al., 1998; Malandain et al., 2004; Dubois et al., 2010).

* Corresponding author at: MIRCen-LMN-CNRS-URA 2210, CEA-DSV-I2BM, 18 route du Panorama, F-92265 Fontenay Aux Roses Cedex, France. Fax: +33 1 46 54 84 51.
E-mail address: thierry.delzescaux@cea.fr (T. Delzescaux).

1053-8119/$ – see front matter © 2011 Elsevier Inc. All rights reserved.
doi:10.1016/j.neuroimage.2011.04.059

Second, the manual delineation of ROIs is labor intensive, time consuming and subject to intra/inter-operator bias. This task can be facilitated by registering digital 3D atlases such as MRI-based atlases to 3D-reconstructed autoradiographic data as we have previously proposed in Lebenberg et al. (2010). This type of analysis enables the rapid evaluation of mean activity levels in atlas-based ROIs.

Third, ROI-based analysis can lead to misinterpretation if opposing effects occur within a single structure (Poldrack, 2007; Dubois et al., 2010). A voxel-wise approach can be taken to avoid the bias caused by an ROI-based approach. This method is based on the statistical comparison of groups of images at the single-voxel scale, and yields "clusters of voxels" that represent functional changes for a given statistically significant level. Such an approach has been developed for clinical studies (Friston et al., 1991, 1995) and can be carried out with the aid of dedicated software such as Statistical Parametric Mapping (SPM) software (Wellcome Department of Imaging Neuroscience, London, UK). However, few *post mortem* functional studies on rodent models have yet been performed with SPM (Nguyen et al., 2004; Lee et al., 2005; Dubois et al., 2008, 2010). In this software, voxel coordinates correspond to a human template such as the Talairach atlas (Talairach and Tournoux, 1988; Lancaster et al., 2000) or the template created by the Montreal Neurological Institute (Collins et al., 1994). The indexation of metabolic changes in anatomical regions in rodents is similarly performed by an expert who superimposes images of clusters onto anatomical images such as Nissl-stained images (Dubois et al., 2010). This operator-dependent and time-consuming task can rapidly become tedious if many clusters are detected, leading to misinterpretation. A recent adaptation of SPM, SPMMouse, is dedicated to small animal imaging and has been used in a morphometric study of transgenic mice (Sawiak et al., 2009). As in the rat studies presented by Schweinhardt et al. (2003) and Casteels et al. (2006), the localization of clusters is indicated by their coordinates with respect to bregma based on anatomical atlases, and defined for the study-specific template. This approach requires anatomical landmarks on the skull to be manually identified and reported to the brain, a difficult task that only yields an approximate localization of clusters (Chan et al., 2007). The clusters thus detected also have to be visually identified by superimposing results derived from the voxel-wise analysis onto anatomical images (Sawiak et al., 2009). In addition, the voxel-wise analysis often suffers from the large number of voxels to be computed, especially with high-resolution autoradiography, which provides a lot of false positive results. A possible partial solution to this problem is the use of the False Discovery Rate (FDR) proposed by Benjamini and Hochberg (1995) and recommended by Frackowiak et al. (2003), in studies dealing with a limited number of subjects. Genovese et al. have proposed this correction to be applied only to a subset of voxels (like voxels located either outside the brain or within the ventricles, where no relevant activity is expected), removing from the analysis any previously disproved hypotheses (Genovese et al., 2002).

The present study proposed to overcome the above-cited limitations and exploit the advantages of both the atlas-based and voxel-wise approaches by combining the two methods of analysis in the mouse brain. We first automatically indexed the results of the voxel-wise approach using an MRI-based atlas, and then used atlas-based segmentation to constrain statistical analysis, a technique commonly known as "*small-volume correction*". The use of an atlas to automatically index clusters of voxels detected by a voxel-wise approach has already been realized in humans (Tzourio-Mazoyer et al., 2002; Eickhoff et al., 2005; Lehericy et al., 2006). The restriction of the statistical analysis using segmented regions has been carried out in human studies using spheres, manual delineation, ROIs defined by cytoarchitectonic probabilistic maps or automatically created using the Talairach Daemon (Maldjian et al., 2003; Eickhoff et al., 2006; Mevel et al., 2007). Dubois et al. have manually segmented brain structures to correct the statistical results of their rat study (Dubois et al., 2008). They, as well as Maheswaran et al., have also proposed the use of digital atlas-based segmentation instead of manual delineation (Maheswaran et al., 2009a; Dubois et al., 2010). To our knowledge, the adjustment of the voxel-wise approach using an atlas in mouse studies has only been suggested in these works but never carried out.

Based on the method described in Lebenberg et al. (2010), we proposed a specific co-registration strategy to fit atlas-based anatomical information to voxel-wise space. The reliability of our approach was assessed qualitatively and quantitatively by comparing atlas-based and manually segmented regions. The method was developed and tested in a preliminary study on a transgenic mouse model of AD ($APP_{SL}/PS1_{M146L}$). The functional dataset used in this study has been analyzed in previous studies using, on the one hand, a voxel-wise approach (Dubois et al., 2010), and on the other hand, an MRI-based atlas approach (Lebenberg et al., 2010). Here, we assessed the relevance of combining the two approaches by comparing the functional parameters yielded using this new approach with results previously described in the literature.

Materials and methods

Biological data

Animals

Our method was applied to four $APP_{SL}/PS1_{M146L}$ mice (64 ± 1 weeks old) and three control $PS1_{M146L}$ littermates (65 ± 2 weeks old), with a C57Bl/6 genetic background. $PS1_{M146L}$ littermates are amyloid-free and were used as controls for $APP_{SL}/PS1_{M146L}$ mice (Delatour et al., 2006). Supplementary details concerning the $APP_{SL}/PS1_{M146L}$ transgenic mouse model of Alzheimer's disease are described in Blanchard et al. (2003). All procedures were carried out in accordance with the recommendations of the EEC (directive 86/609/EEC) and the French National Committee (decree 87/848) for the use of laboratory animals.

Data acquisition

[^{14}C]-2-deoxyglucose (2-DG) was injected *in vivo* to evaluate cerebral glucose uptake in mouse brains by quantitative autoradiography. Additional details of 2-DG experiments are described in Hérard et al. (2005), with the exception that in our study, animals were awake but non-stimulated. Glucose uptake was measured only in the right hemisphere, which was extracted following euthanasia for *ex situ* analysis and cut into 20 μm-thick serial coronal sections in a cryostat. The non-subcortical part of the olfactory bulb and cerebellum were excluded (see top left of Fig. 1). Every fourth serial section was mounted on a Superfrost glass slide and exposed to autoradiographic film, together with radioactive [^{14}C] standards. The same sections were also processed for Nissl staining in order to obtain anatomical information. Images from the brain surface, corresponding to the sections processed, were recorded prior to sectioning using a digital camera with an in-plane resolution of $27 \times 27 \mu m^2$. Technical details concerning imaging systems used to acquire the above data are more largely described in Dubois et al. (2010) and in Lebenberg et al. (2010).

3D-reconstructed multimodal post mortem data

Autoradiographs and histological sections were digitized as 8-bit grayscale images using a flatbed scanner with a 1200 dpi in-plane resolution (pixel size $21 \times 21\ \mu m^2$). Using BrainRAT (toolbox of the free software BrainVISA, http://brainvisa.info/) and the method presented in Dubois et al. (2010), three spatially coherent 3D-reconstructed *post mortem* volumes were obtained for each mouse with a common frame of reference: one block-face volume ($350 \times 308 \times 120$ array with a resolution of $27 \times 27 \times 80\ \mu m^3$), one autoradiographic, and one histological volume each ($479 \times 420 \times 120$ array with a resolution of $21 \times 21 \times 80\ \mu m^3$).

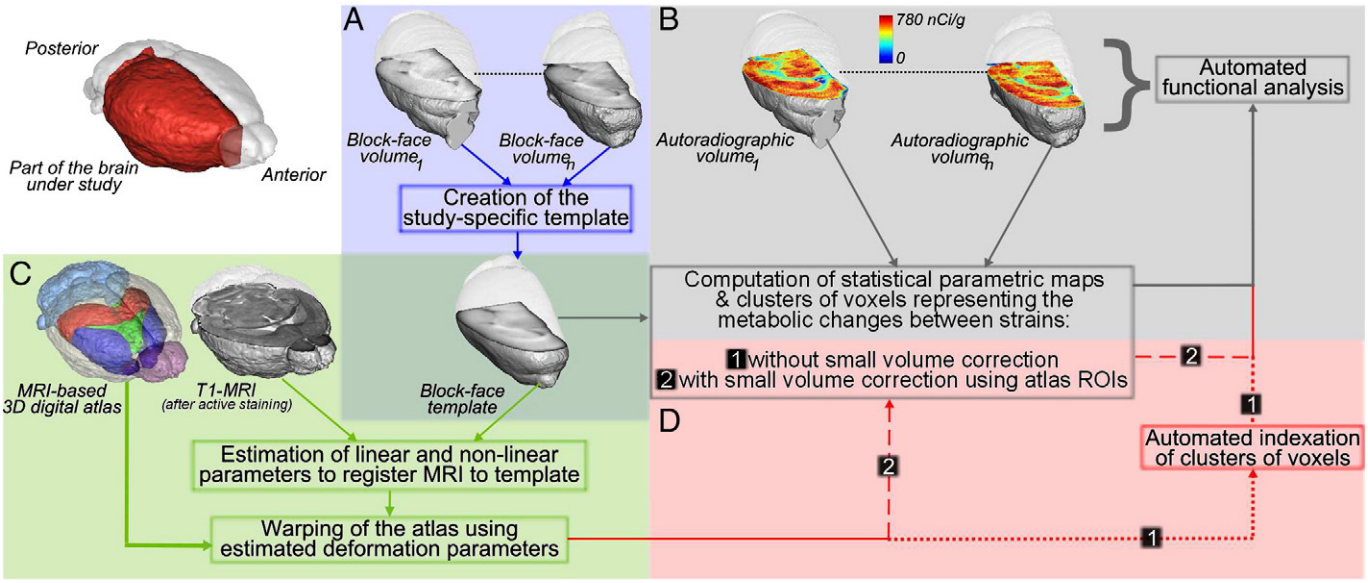

Fig. 1. Overview of our method to automatically index and analyze metabolic changes detected by a voxel-wise approach using an MRI-based digital atlas: the left top part of the figure represents the part of the brain under study in 3D (subvolume in red); (A) creation of a study-specific template based on block-face volumes; (B) computation of statistical parametric maps from 3D-reconstructed autoradiographic volumes of the dataset to provide clusters of voxels displaying metabolic changes between strains and automated analysis of functional volumes of the dataset; (C) registration of an MRI-based digital atlas to the study-specific template followed by the superimposition of the registered atlas on statistical parametric maps; (D) automated indexation of clusters of voxels without (D1) and with (D2) small-volume correction and automated analysis of functional volumes of the dataset using the indexed clusters.

MRI-based 3D digital mouse brain atlas

Data acquisition

The MRI-based 3D digital atlas used for our study was downloaded from the Website of the Center for *In Vivo* Microscopy (http://www.civm.duhs.duke.edu/) and is currently available at the Biomedical Informatics Research Network (BIRN) Data Repository (BDR) (https://bdr-portal.nbirn.net/). This atlas was derived from T1 and T2-weighted 3D MR images (9.4 T) of one young adult (9–12 weeks) C57Bl/6 J mouse (same genetic background as our animals). To enhance image quality, and preserve *in vivo* geometry, MR images were acquired *in situ*, *i.e.* within the cranial vault, after active staining of the brain (Johnson et al., 2007; Badea et al., 2007; Dorr et al., 2008). T2-weighted MRI was processed using the MEFIC method (Sharief and Johnson, 2006). The isotropic scan resolutions were 21.5 μm (T1) and 43 μm (T2) using $512\times512\times1024$ and $256\times256\times512$ arrays respectively. Thirty-three anatomical structures were semi-automatically segmented as described in Sharief et al. (2008).

Data post-processing

To enable the study of the biological data, the MRI and atlas volumes were reoriented as described in Prima et al. (2002) to realign the interhemispheric plane with our referential axes. The hemisphere to be studied was thus automatically extracted. We then interactively cropped the MRI to select (and preserve) the part of the hemisphere to be registered (excluding the cerebellum and olfactory bulb in the present work). The atlas volume was automatically cropped using parameters determined previously.

The work described in Dubois et al. (2010) highlighted metabolic changes between the two groups of animals in the cingulate and retrosplenial cortex. This anterior part of the cortex was not segmented in the MRI-based digital atlas. This region was therefore manually segmented by a neuroanatomist from the original MRI-based atlas segment delineating the whole cortex and using the T1-weighted MRI contrast. It added to the ROI list in order to confirm metabolic changes in this area.

Detection of metabolic changes using a voxel-wise approach

Creation of a study-specific template and spatial normalization of autoradiographic volumes

The detection of metabolic changes in mouse brains was performed using the SPMMouse extension of the 5th version of the Statistical Parametric Mapping software (SPM5: Wellcome Department of Imaging Neuroscience, London, UK) dedicated to the study of images from small animal brains (Sawiak et al., 2009). To analyze 3D-reconstructed autoradiographic data, a study-specific template based on block-face volumes was first created (Fig. 1A) using a protocol described previously (Nguyen et al., 2004; Dubois et al., 2008) : 1) one block-face volume has been chosen as reference for the study-specific template, 2) the image was smoothed using a Gaussian kernel so that the FWHM was equal to 3 times the voxel size of the data ($81\times81\times240$ microns), 3) all block-face volumes were then spatially normalized to this smoothed data using linear and nonlinear transformations implemented using the SPMMouse software, 4) an average volume was created from spatially normalized block-face volumes and 5) the mean image was smoothed using the same filter as the one used previously. Autoradiographic volumes were then spatially normalized to this template using linear and nonlinear transformations implemented using the same software. To measure glucose uptake, gray-level intensities of the spatially normalized autoradiographic volumes were calibrated using co-exposed [^{14}C] standards and converted into activity values (nCi/g). Corrective coefficients were applied to normalize global brain activity so as to allow comparison between strains (Valla et al., 2006). Finally, functional data were smoothed using a Gaussian kernel so that the FWHM was equal to 3 times the voxel size of the data ($63\times63\times240$ microns).

Statistical design in SPMMouse

Using a two-sample *t*-test, two contrasts were evaluated independently to produce statistical parametric maps from the gray-level intensities of autoradiographic volumes: 1) voxels with a lower 2-DG

uptake in APP/PS1 mice than in PS1 controls (APP/PS1 hypometabolism), and 2) voxels with a higher 2-DG uptake in APP/PS1 mice than in PS1 controls (APP/PS1 hypermetabolism) (Fig. 1B). The background and ventricles were subtracted from the analysis using a pre-specified threshold: only had been kept the voxels whose intensity, in all the images, was at least equal to 80% of the average intensities of image voxels. As in a previous study (Dubois et al., 2010), clusters of voxels representing metabolic changes were determined using $P<0.01$ (uncorrected for multiple comparisons) as the level of statistical significance. Each cluster contained at least 1500 contiguous voxels (cluster size $\gtrsim 0.05\ mm^3$).

Evaluation of metabolic changes displayed by the clusters

The average uptake of 2-DG (nCi/g, mean ± SEM, with SEM the associated standard error of the mean) was measured in autoradiographic volumes from all APP/PS1 and PS1 mice for each cluster detected by the voxel-wise approach. Measurement was carried out using functions implemented in C++ using in-house software. The percentage of metabolic differences between strains was calculated from these values for each brain structure.

Automated indexation of detected clusters using the digital atlas

Registration of the digital atlas to the study-specific template

Digital atlas-based segmentation was used to automatically localize the clusters of voxels detected by the voxel-wise analysis. As statistical parametric maps were in the same frame of reference as the study-specific template, we first linearly registered the T1-weighted MRI to the study-specific template based on block-face volumes, using rigid and affine transformations as described in Lebenberg et al. (2010). A nonlinear deformation, initialized using the previously estimated transformation, was then carried out using the Free Form Deformation method to locally enhance MRI and template registration (Rueckert et al., 1999; Mattes et al., 2003). The MRI and the corresponding digital atlas were then warped using the final estimated transformation. This strategy is illustrated in Fig. 1C. The mathematical algorithms were all implemented in C++ using in-house software. BrainVISA pipelines were developed in Python to link registration steps with limited operator intervention.

Evaluation of registration

Registration accuracy was qualitatively assessed by a visual inspection of the superimposition of the inner and outer contours of registered MRI (extracted using a Deriche Filter (Deriche, 1987)) on a 3D-reconstructed histological volume of the dataset, spatially normalized to the study-specific template using linear and nonlinear transformations implemented in SPMMouse.

To quantitatively evaluate data registration, the superimposition between atlas-based segmentation and ROIs manually delineated within the histological volumes was measured using overlap criteria. The hippocampus, cortex, striatum (merging of the accumbens nucleus and caudate putamen ROIs), corpus callosum and substantia nigra were manually delineated in one Nissl-stained APP/PS1 and one PS1 mouse brain. Block-face volumes corresponding to these histological volumes were spatially normalized to the study-specific template using linear and nonlinear transformations implemented in SPMMouse. The estimated deformation parameters were applied to the manual delineations to register them to the study-specific template. Volume differences, sensitivity and Dice coefficients (Dice, 1945) between registered atlas-based and manual ROIs were computed as overlap criteria. It should be noted that a Dice coefficient greater than 0.7 is considered in the literature to indicate a good level of concordance between the two types of segmentation (Zijdenbos et al., 1994). An overview of the method established to quantitatively evaluate data registration is illustrated in Fig. 2.

Classification of detected clusters within atlas-based segments

The registered atlas was superimposed onto statistical parametric maps. A visual evaluation enabled the direct indexation of the clusters detected within anatomical regions segmented in the digital atlas.

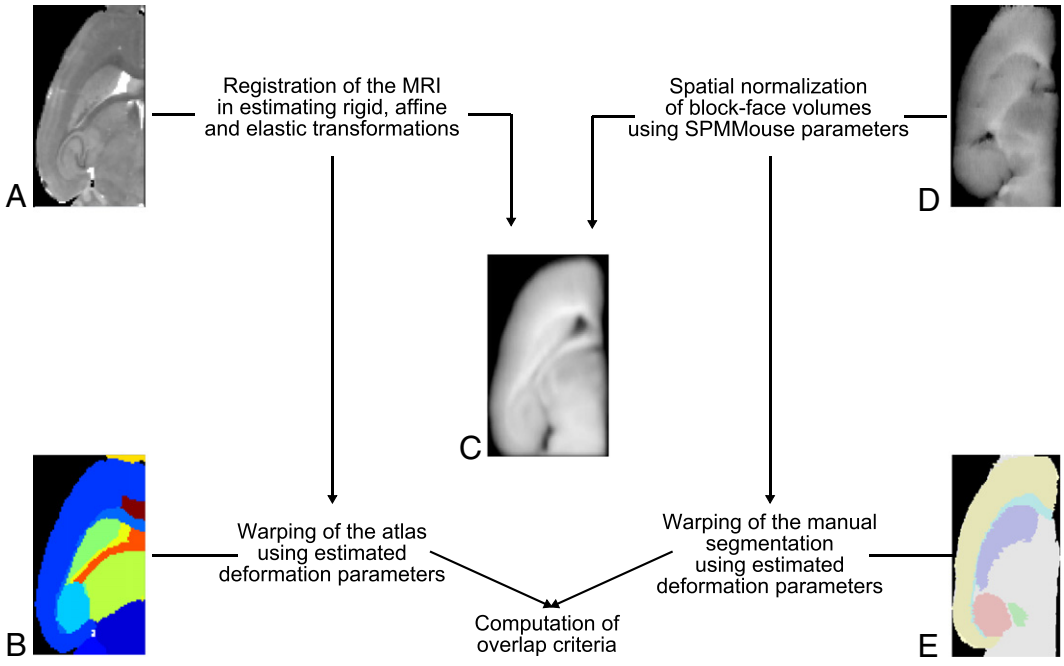

Fig. 2. Overview of the method to quantitatively evaluate the registration of the digital atlas to the study-specific template: estimation of rigid, affine and elastic transformations to register (A) the MRI to (C) the study-specific template; deformation of (B) the atlas using parameters previously estimated; spatial normalization of (D) the block-faces volumes to (C) the study-specific template; deformation of (E) the manual segmentation using parameters previously estimated. Overlap criteria were calculated between deformed atlas-based and manual segments.

Volumetric and functional analysis of metabolic changes classified according to atlas-based segmentation

Overlap rate between detected clusters and atlas-based segments

Clusters representing metabolic changes were automatically classified within atlas-based ROIs according to their degree of overlap (Fig. 1D-1). The distribution of clusters in the mouse hemibrain was analyzed by computing the percentage of cluster voxels that overlapped with ROI voxels, as previously performed in humans (Tzourio-Mazoyer et al., 2002; Eickhoff et al., 2005). As clusters of voxels can be spread over several ROIs, we computed the volumes of each part of a cluster automatically indexed to a given atlas-based segment (called a *subcluster*) to confirm that it belonged to the anatomical region in question and exclude potential atlas misregistration to the study-specific template. We assumed that all subclusters smaller than 0.05 mm^3 were due to atlas misregistration. A visual inspection of the superimposition of clusters with atlas-based segments and with histological volumes was carried out to confirm this assumption.

Functional analysis of clusters spread over several atlas-based segments

The significant spreading of a cluster over several atlas-based segments could be due to the statistical inferences presets built into SPMMouse. In this case, we assumed that some clusters were the result of the merging of separate but smaller clusters, and that the average 2-DG uptake of autoradiographic volumes would therefore be different in subclusters extracted from a "single" cluster between APP/PS1 and PS1 mice. We thus measured average 2-DG uptakes (nCi/g, mean ± SEM) in each subcluster and the percentage of metabolic differences between strains calculated from these values.

Small-volume correction using the registered digital atlas

The statistical design described above can lead to a large number of false positives in statistical parametric maps ($P \times n$, where P is the statistical significance level chosen and n the number of voxels detected as positive for the statistical test). To reduce the proportion of false positives compared to the total number of activated voxels, we reduced the number of tests realized simultaneously using atlas-based ROIs, and then applied the FDR correction to the selected parts of the images.

Statistical analysis based on the two-sample t-test was also constrained by successively using each registered atlas-based segment as an explicit mask in the statistical design in SPMMouse (Fig. 1D-2). The two types of contrast (APP/PS1 hypo- and hypermetabolism) were again evaluated using the FDR correction, taking $P<0.05$ as the level of statistical significance and without any restriction on the minimum number of contiguous voxels (extend threshold = 0).

Due to the reduced number of subjects involved, the results obtained must be considered as preliminary.

Results

Detection of metabolic changes using a voxel-wise approach

Estimated statistical parametric maps taking $P<0.01$ (uncorrected for multiple comparisons) as to be the level of statistical significance and containing at least 1500 contiguous voxels yielded 9 clusters showing hypometabolism in APP/PS1 mice and 8 showing hypermetabolism. Fig. 3 displays in 3D (A and B) and in 2D (C and D) these regions of lower and higher 2-DG uptake in APP/PS1 when compared to PS1 mice. As shown in this figure, areas of hypometabolism in APP/PS1 mice occupied a larger volume than those of hypermetabolism in the brain of these animals. We also observed that areas with differences in metabolism between strains were distributed throughout the hemisphere. Finally, this figure illustrates the challenge posed by the classification of clusters into anatomical ROIs, even with the help of an atlas such as the one presented by (Paxinos and Franklin, 2001).

Table 1 indicates the average 2-DG uptake (nCi/g, mean±SEM) of each group and the percentage of metabolic differences between strains. Clusters were assigned arbitrary numbers for identification. Table 1A shows that the average activity of clusters in which there was hypometabolism was ~19% lower in APP/PS1 than in PS1 mice. Within clusters representing hypermetabolism (Table 1B), the average activity was ~26% higher in APP/PS1 than in PS1 mice.

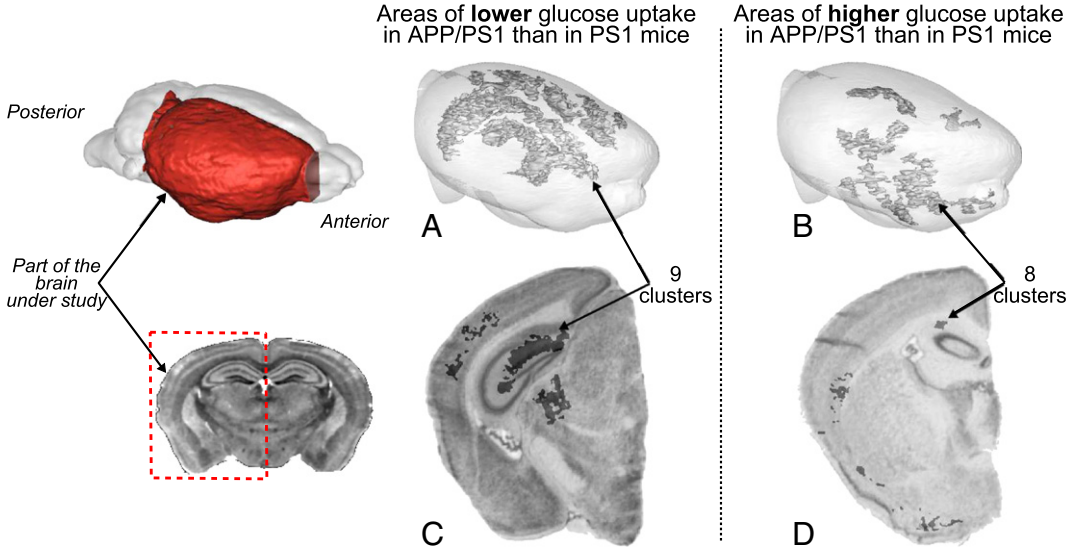

Fig. 3. The left part of the figure represents the part of the brain under study in 3D (subvolume in red at the top) and in 2D (in the red dotted rectangle at the bottom). (A and B) 3D and (C and D) 2D representations of clusters of voxels yielded by voxel-wise analysis (in gray), revealing areas of lower and higher glucose uptake in APP/PS1 than in PS1 mice.

Table 1
Quantification of hypo- (A) and hypermetabolism (B) in APP/PS1 mice and percentage of difference between APP/PS1 and PS1 mice (results of the voxel-wise analysis using $P<0.01$ uncorrected for multiple comparisons and extent threshold = 1500).

No. of cluster	PS1 mice (n = 3) $\overline{\mu_{act}} \pm$ SEM (nCi/g)	APP/PS1 mice (n = 4) $\overline{\mu_{act}} \pm$ SEM (nCi/g)	% diff between groups
(A) Clusters showing lower glucose uptake areas in APP/PS1 than in PS1 mice			
1	307.22 ± 1.80	255.01 ± 0.49	− 16.99
2	366.22 ± 13.88	275.88 ± 2.97	− 24.67
3	319.97 ± 3.86	270.24 ± 3.49	− 15.54
4	320.78 ± 2.64	265.28 ± 1.15	− 17.30
5	333.07 ± 9.39	264.88 ± 1.74	− 20.47
6	302.83 ± 3.24	241.31 ± 2.40	− 20.31
7	282.91 ± 2.52	228.37 ± 2.94	− 19.28
8	336.98 ± 6.09	275.56 ± 2.24	− 18.23
9	338.87 ± 3.66	281.03 ± 5.85	− 17.07
(B) Clusters showing higher glucose uptake areas in APP/PS1 than PS1 mice			
1	171.28 ± 14.48	278.26 ± 6.22	+ 62.46
2	240.33 ± 2.34	283.98 ± 2.21	+ 18.16
3	256.06 ± 0.55	309.03 ± 4.13	+ 20.69
4	238.51 ± 2.05	294.80 ± 2.17	+ 23.60
5	190.77 ± 3.97	238.39 ± 2.33	+ 24.97
6	260.64 ± 1.87	297.08 ± 1.86	+ 13.98
7	272.08 ± 7.02	345.86 ± 7.08	+ 27.12
8	209.88 ± 2.25	247.63 ± 1.58	+ 17.99

Comparison of mean activity ($\overline{mean} \pm$ SEM (nCi/g)) measured in clusters of voxels resulting from the voxel-wise approach. For clusters displaying hypo- (A) and hypermetabolism (B) in APP/PS1 mice, the percentage of difference between APP/PS1 and PS1 mice was computed. Average activity within clusters representing hypometabolism was ~19% lower in APP/PS1 than in PS1 mice. Within clusters/subclusters representing hypermetabolism, the average activity was ~26% higher in APP/PS1 than in PS1 mice.

Automated indexation of detected clusters using the digital atlas

Digital atlas and study-specific template registration

Visual inspection indicated the good registration of MRI-based inner structures (such as the hippocampus and corpus callosum) and external contours to a 3D-reconstructed histological volume of the dataset, spatially normalized to the study-specific template (see Fig. 4). Deformation grids, illustrated in Fig. 4C, show that nonlinear transformation homogeneously deformed MR images to register this volume to the block-face template.

Table 2 displays volume differences, Dice coefficients and sensitivity computed for the atlas-based and manual segmentation of the cortex, corpus callosum, hippocampus, striatum and substantia nigra of one PS1 and one APP/PS1 mouse, registered to the study-specific template as described in Fig. 2. Volume difference scores show that the atlas enabled the volume of the cortex to be evaluated from the block-face template with a mean error of 5% (corresponding to ~4 mm^3 per hemisphere), the corpus callosum with a mean error of 14% (~1 mm^3 per hemisphere), the hippocampal volume with a mean error of 12% (~2 mm^3 per hemisphere), striatal volume with a mean error of 8% (~1 mm^3 per hemisphere) and the volume of the substantia nigra with a mean error of 7% (~0.1 mm^3 per hemisphere). Dice coefficients and sensitivity indices obtained for large structures (~0.79 and ~0.77 resp.) were higher than those obtained for small or thin ROIs such as the corpus callosum or the substantia nigra ($\overline{\kappa}$ ~0.45 and $\overline{Se}$ ~0.43).

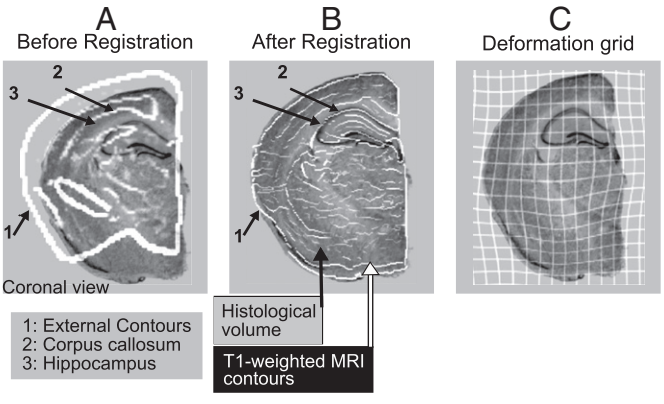

Fig. 4. Superimposition of the contours of the T1-weighted MR image (in white) on one 3D-reconstructed histological volume spatially normalized to the study-specific template, before (A) and after (B) the registration process. The external contours (1) and those defining inner structures such as the corpus callosum (2) and the hippocampus (3) visually attest to the successful registration of the two types of data (B). Deformation grids (C) show that the nonlinear transformation homogeneously deformed the MRI to register this volume to the block-face template.

Automated classification of detected clusters within the mouse brain

To automatically classify clusters of voxels within cerebral structures, the registered atlas was superimposed onto statistical parametric maps. Visual inspections carried out using 2D views such as those illustrated in Fig. 5 enabled the direct indexation of detected clusters within anatomical ROIs: clusters observed in Fig. 5A belonged to the retrosplenial and cingulate cortex, the "rest of the cortex" (*i.e.* the cortex excluding the retrosplenial and cingulate regions), the hippocampus or the thalamus. Clusters detected for this contrast type (hypometabolism) were also assigned to the brainstem, the cerebellum, the corpus callosum, the inferior and superior colliculi, the internal capsule, the merging of the septum and the fimbria, the striatum and the ventricles. The clusters observed in Fig. 5B were indexed within the "rest of the cortex" and the hippocampus. An inspection of the rest of the results obtained for this second contrast type (hypermetabolism) revealed clusters in the amygdala, the anterior commissure, the corpus callosum, the olfactory bulb and the striatum.

These observations reveal that clusters displaying metabolic changes between APP/PS1 and PS1 mice can be spread over several anatomical structures (white circle in Fig. 5A). Figs. 6A and B illustrate 3D clusters displaying hypo- and hypermetabolism respectively in APP/PS1 mice, and which are undoubtedly spread over several ROIs.

Volumetric and functional analysis of metabolic changes classified within atlas-based segments

Overlap rate between detected clusters and atlas-based segments

Table 3 presents the rate of overlap between the clusters detected and atlas-based segments. Table 3A shows that 3 of the 9 clusters displaying hypometabolism in APP/PS1 mice were entirely included in the ROI called the "rest of the cortex" (clusters 3, 8 and 9). Of the 8 clusters displaying hypermetabolism in APP/PS1 mice, 1 was also entirely included in this ROI (cluster 1).

Based on these rates, we were able to automatically compute the volume of each subcluster belonging to a specific structure. All subclusters smaller than 0.05 mm^3 (minimum cluster size required by

Table 2
Computation of overlap criteria for 5 ROIs of one PS1 and one APP/PS1 mouse.

	PS1 mouse (ctrl)			APP/PS1 mouse (AD model)		
	Δ_V	κ	Se	Δ_V	κ	Se
Cortex	0.06	0.83	0.86	0.04	0.74	0.73
Corpus callosum	0.27	0.55	0.49	0.01	0.31	0.31
Hippocampus	0.16	0.83	0.77	0.08	0.75	0.72
Striatum	0.12	0.83	0.78	0.04	0.75	0.77
Substantia nigra	0.11	0.42	0.40	0.02	0.52	0.52

Volume difference (Δ_V), Dice coefficient (κ) and Sensitivity (Se) computed for the cerebral cortex, corpus callosum, hippocampus, striatum and substantia nigra of one PS1 and one APP/PS1 mouse registered to the study-specific template, to evaluate the concordance between registered atlas-based and manually delineated ROIs. Final mean scores show that the atlas assigned most voxels to the appropriate structure.

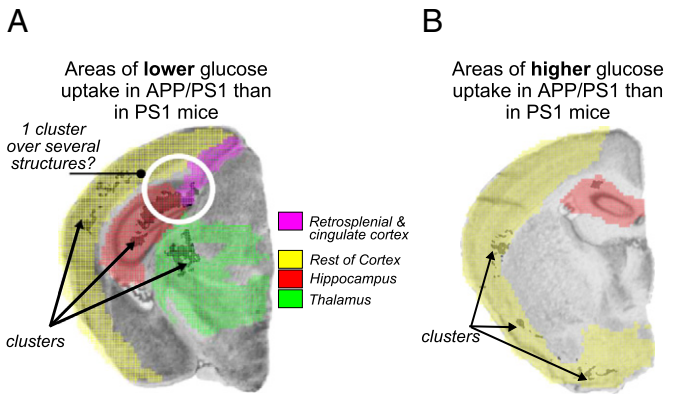

Fig. 5. Fusion of registered atlas-based segments, clusters detected with lower (A) and higher (B) glucose uptake in APP/PS1 than in PS1 mice, and histological data spatially normalized to the block-face template. The white circle in (A) shows that one cluster can be spread over several anatomical structures.

the statistical design) were considered to be the consequence of atlas misregistration and excluded from subsequent analysis. Clusters 1, 2 and 5 which displayed hypometabolism in APP/PS1 mice, were thus automatically reclassified within the striatum, the retrosplenial and cingulate cortex, and the thalamus, respectively. Clusters 2, 3 and 6 which displayed hypermetabolism in APP/PS1 mice, were automatically indexed in the "rest of the cortex". Cluster 8, detected in the latter contrast group, was automatically assigned to the amygdala.

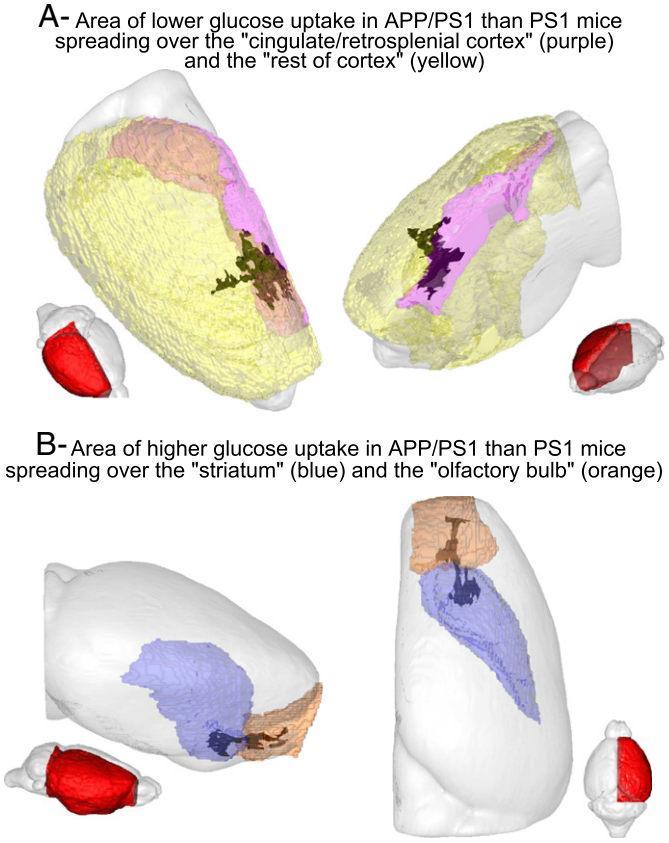

Fig. 6. 3D representation of clusters of voxels displaying metabolic differences between APP/PS1 and PS1 mice and spread over several anatomical structures: in (A), a cluster of voxels showing hypometabolism in APP/PS1 mice and belonging to the atlas-based ROIs "cingulate/retrosplenial cortex" (purple) and "rest of cortex" (yellow); in (B), a cluster of voxels displaying hypermetabolism in APP/PS1 mice and spreading over the "striatum" (blue) and the "olfactory bulb"(orange).

One cluster belonging to the ventricles (cluster 7, APP/PS1 hypometabolism) was also considered to be misregistered, since the ventricles had been subtracted from the analysis beforehand. After visual inspection, the concerned part of this cluster was merged with the closest ROI, *i.e.* the striatum, for functional analysis.

Only the overlapping areas highlighted in gray in Table 3 were included in the subsequent analysis. A 3D representation of atlas-indexed clusters is displayed in Fig. 7.

Functional analysis of clusters spread over several atlas-based segments

Table 4 compares the activity per group measured in each subpart of clusters spread over several atlas-based ROIs.

In Table 4A:

- *Glucose uptake measured in subparts of cluster 4.* Results show that the percentage of metabolic difference between strains was 2 points greater for the subcluster assigned to the "cingulate and retrosplenial cortex" than for the subcluster classified within the ROI "rest of the cortex".
- *Glucose uptake measured in subparts of cluster 6.* The table shows that the percentage of metabolic difference between strains was 2 points lower for the subcluster indexed within the ROI "rest of the cortex" than for the subcluster classified within the hippocampus and the cingulate and retrosplenial cortex.

In Table 4B:

- *Glucose uptake measured in subparts of cluster 4.* Activity measured in the subcluster assigned to the olfactory bulb was lower than that measured in the subcluster indexed within the striatum. In addition, the percentage of metabolic difference between strains for the first subcluster was 10 points higher than for the second subcluster.
- *Glucose uptake measured in subparts of cluster 5.* Results show that the activity measured in the subcluster classified within the corpus callosum was lower than in the subcluster indexed within the hippocampus. The percentage of metabolic difference between strains computed for the first subcluster was more than 3 points higher than for the second subcluster.
- *Glucose uptake measured in subparts of cluster 7.* The table shows that activity measured in the subcluster classified within the cortex was similar to that measured in the subcluster indexed within the striatum.

Small-volume correction using the registered digital atlas

Statistical analysis of the results indicated above was constrained by successively using each registered atlas-based segment as an explicit mask in the statistical design of SPMMouse. This enabled the number of voxels tested to be reduced by a factor of 10 or 100.

Only the application of the hippocampal mask onto functional data permitted an FDR correction of the statistical analysis for the contrast "APP/PS1 hypometabolism", considering $P<0.05$ as the level of statistical significance and without any restriction on the minimum number of contiguous voxels. The percentage of metabolic difference between strains was estimated around ~-22.39%, *i.e.* 2 points higher than that computed for the subcluster indexed within the hippocampus (see Table 4A).

Fig. 8 illustrates the hippocampal area of lower glucose uptake in APP/PS1 than in PS1 mice, obtained with (dark red) and without (light red) correction for multiple comparisons. The area yielded by the constrained analysis was ~0.74 mm^3, compared to the unrestricted area of ~1.39 mm^3.

Table 3
Percentage of cluster voxels overlapping with atlas-ROI voxels.

(A) Clusters showing lower glucose uptake areas in APP/PS1 than in PS1 mice

Atlas–based ROIs	No. and *volume* of the cluster (mm^3)								
	1	**2**	**3**	**4**	**5**	**6**	**7**	**8**	**9**
	0.33	*0.50*	*0.05*	*0.46*	*1.36*	*1.65*	*0.23*	*0.50*	*0.08*
Brainstem	–	–	–	–	0.06	0.01	–	–	–
Cerebellum	–	–	–	–	–	0.01	–	–	–
Cing./retro. cortex	–	98.49	–	72.17	–	2.86	–	–	–
Rest of cortex	9.23	0.10	100	27.69	–	9.97	0.15	100	100
Corpus callosum	1.42	1.41	–	0.14	–	0.02	1.69	–	–
Hippocampus	–	–	–	–	–	84.41	–	–	–
Inf. colliculus	–	–	–	–	–	1.16	–	–	–
Internal capsule	–	–	–	–	–	–	0.60	–	–
Septum/fimbria	–	–	–	–	–	–	1.83	–	–
Striatum	89.36	–	–	–	–	–	51.04	–	–
Sup. colliculus	–	–	–	–	–	1.49	–	–	–
Thalamus	–	–	–	–	99.94	0.09	–	–	–
Ventricles	–	–	–	–	–	–	44.68	–	–

(B) Clusters showing higher glucose uptake areas in APP/PS1 than PS1 mice

Atlas–based ROIs	No. and *volume* of the cluster (mm^3)							
	1	**2**	**3**	**4**	**5**	**6**	**7**	**8**
	0.06	*0.29*	*0.18*	*0.17*	*0.33*	*0.07*	*0.39*	*0.13*
Amygdala	–	0.24	5.13	–	–	–	–	73.41
Ant. commissure	–	–	–	5.37	–	–	–	–
Corpus callosum	–	0.71	–	–	25.17	20.26	–	–
Rest of cortex	100	99.05	91.54	1.87	0.43	79.09	77.13	26.49
Hippocampus	–	–	–	–	74.40	–	–	–
Olf. bulb	–	–	–	45.43	–	–	–	–
Striatum	–	–	3.33	47.33	–	0.65	22.87	0.10

Computation of percentage of cluster voxels showing hypo- (A) and hypermetabolism (B) in APP/PS1 mice overlapping with atlas-ROI voxels (results obtained with $P<0.01$ uncorrected for multiple comparisons and an extent threshold = 1500 voxels). Whereas some clusters of voxels were entirely included within a single ROI, others were spread over several anatomical structures. Among the latter, only subclusters greater than 0.05 mm_3 (minimum cluster size required for the statistical design) were considered for subsequent analysis (high-lighted in gray). Since the ventricles were subtracted from the statistical analysis, the subcluster classified in this ROI (in A) was merged with the closest subcluster, *i.e.*, the one indexed in the striatum.

Discussion

The main goal of this study was to improve on the atlas-based and voxel-wise approaches used individually for the analysis of *post mortem* mouse brain functional images, by proposing a more efficient combined approach.

The usual method to study these images uses an ROI-based approach carried out with 2D sections. To overcome the limitations caused by numerous manual delineations, we previously registered a 3D digital MRI-based atlas to 3D-reconstructed functional data (Lebenberg et al., 2010). However, such an analysis may fail if areas with variations are small in comparison with the size of ROIs, or if opposing effects occur within a single structure (Poldrack, 2007). Other approaches such as voxel-wise analysis have been tested to detect local functional changes and have revealed areas of hypo- and hypermetabolism within a single structure (Dubois et al., 2010). However, the localization and anatomical identification of areas displaying changes still need time-consuming expert intervention (see Fig. 3).

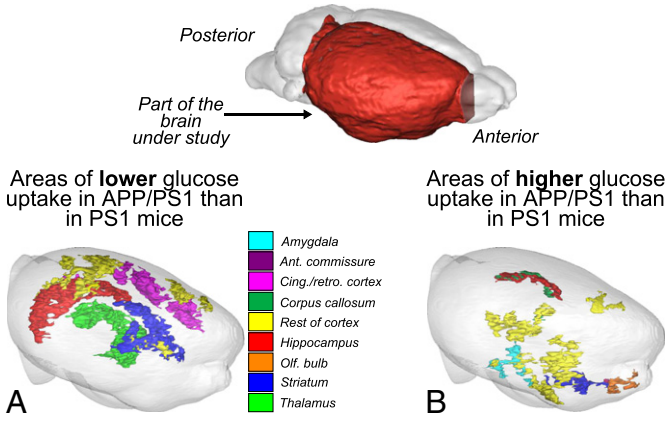

Fig. 7. 3D representation of clusters displaying metabolic differences between APP/PS1 and PS1 mice and automatically indexed within various anatomical structures using atlas-based segmentation.

We thus proposed a combination of the advantages offered by the two approaches: 1) functional data were analyzed using a voxel-wise approach to reveal slight metabolic changes, and 2) a digital atlas was used to index these results. As a first step, we sought to spatially analyze the results of the voxel-wise approach using atlas-guided digital mapping. We then constrained the statistical analysis using atlas-based segmentation. Two aspects of this combined approach proved to be challenging. The first was to validate the registration of an MRI-based atlas to the statistical parametric maps that yielded clusters of activated voxels. The second was to evaluate whether small-volume corrections could be applied to the voxel-wise analysis of autoradiographic data from rodents using an MRI-based atlas, and whether such a combination of methods could improve the results obtained from a study with a small number of animals (4 AD mice and 3 control littermates), especially those that had not been previously stimulated or lesioned.

Digital atlas and study-specific template registration

Digital atlas-based segmentation was used to automatically localize clusters detected by the voxel-wise approach. Since the statistical parametric maps generated were in the same frame of reference as the study-specific template, the T1-weighted MRI corresponding to the digital atlas and the atlas-based volume were automatically registered to these maps using the strategy described in Lebenberg et al. (2010), with the block-face template as the reference image.

Visual inspection confirmed that the registration of MRI-defined inner structures and external contours to a 3D-reconstructed histological volume of the dataset spatially normalized to the study-specific template was accurate (see Fig. 4). The quantitative evaluation performed by computing criteria for the overlap of atlas-based segments and manually delineated ROIs (see Table 2) attests that the atlas correctly assigned most voxels to the appropriate structure. The lower scores computed for small and deep ROIs (corpus callosum and substantia nigra) suggest that the identification of these regions should be verified.

These results could be due to the multimodal registration process, since the information contained in one image is not necessarily present in others. Additional registration difficulties surfaced because we registered cropped whole-brain MR images to a smoothed template based on *post mortem* block-face hemibrain images, acquired inside and outside the skull respectively. Cerebral tissue could have been damaged due to handling (some parts of the experimental images could have thus been deformed), and the loss of the meninges and cerebrospinal fluid during brain extraction from the skull and the separation of the hemispheres could have resulted in additional deformation. Some ROIs, such as the ventricles and neighboring structures, especially thin regions like the corpus callosum, could have been misregistered as a consequence of ventricular collapse. This could explain the low overlap scores obtained for this ROI. In addition, the registration strategy was mainly driven by large and noncomplex ROIs at the expense of small and complex anatomical structures, thus weighting the contribution of the ROIs involved to the registration process. The good registration of a leading ROI could thus have generated registration errors in a smaller adjacent area. The smoothing and spatial normalization steps required to create the reference image could also have rendered small and deep ROIs undiscernible on the

Table 4
Comparison of mean activity measured in each subpart of clusters spread over several atlas-based ROIs.

No. of cluster	Atlas-based ROIs	PS1 mice (n=3) $\overline{\mu_{act}} \pm$ SEM (nCi/g)	APP/PS1 mice (n=4) $\overline{\mu_{act}} \pm$ SEM (nCi/g)	% diff between groups
(A) Clusters showing lower glucose uptake areas in APP/PS1 than in PS1 mice				
4	Cing./retro. cortex	318.87 ± 4.32	261.92 ± 1.14	−17.86
	Rest of cortex	326.16 ± 3.02	274.41 ± 1.93	−15.87
6	Cing./retro. cortex	311.03 ± 7.80	247.50 ± 5.13	−20.43
	Rest of cortex	310.38 ± 3.94	254.50 ± 3.48	−18.00
	Hippocampus	301.42 ± 3.21	239.33 ± 3.19	−20.60
(B) Clusters showing higher glucose uptake areas in APP/PS1 than in PS1 mice				
4	Olf. bulb	217.98 ± 4.51	281.99 ± 3.17	+29.37
	Striatum	258.01 ± 0.73	307.11 ± 1.94	+19.03
5	Corpus callosum	180.00 ± 4.21	229.67 ± 2.05	+27.60
	Hippocampus	194.54 ± 3.94	241.54 ± 2.43	+24.16
7	Rest of cortex	271.06 ± 7.63	344.79 ± 7.32	+27.20
	Striatum	275.53 ± 5.63	349.46 ± 6.37	+26.83

The mean activity ($\overline{mean} \pm$SEM (nCi/g)) was measured in each part of a cluster spread over several atlas-based ROIs. For subclusters displaying hypo- (A) and hypermetabolism (B) in APP/PS1 mice, the percentage of difference between APP/PS1 and PS1 mice was computed. Results obtained for clusters 4 and 6 in (A) and for clusters 4 and 5 in (B) show that the activity of each subpart extracted from a cluster was different. Glucose uptake was similar in subparts extracted from the cluster 7 in (B).

representative image. Their localization on the template using the atlas was thus more complex. The use of a probabilistic atlas to segment a template based on block-face volumes may improve registration results, and thus, template analysis.

Automated indexation of detected clusters using the digital atlas

The indexation of metabolic differences between strains of transgenic mice was directly performed by superimposing the registered atlas onto statistical parametric maps. Visual inspections of 2D and 3D images led to the conclusion that clusters displaying metabolic changes between APP/PS1 and PS1 mice could be spread over several anatomical structures (see Figs. 5 and 6). We also noticed that some anatomical structures in APP/PS1 mice displayed both areas with hypometabolism and with hypermetabolism (hippocampus, striatum, corpus callosum and the cortex excluding the cingulate and retrosplenial parts). Interestingly, our approach identified structures such as the olfactory bulb and the corpus callosum as being potentially involved in Alzheimer's disease. This could have been missed with a visual identification of clusters (Dubois et al., 2010).

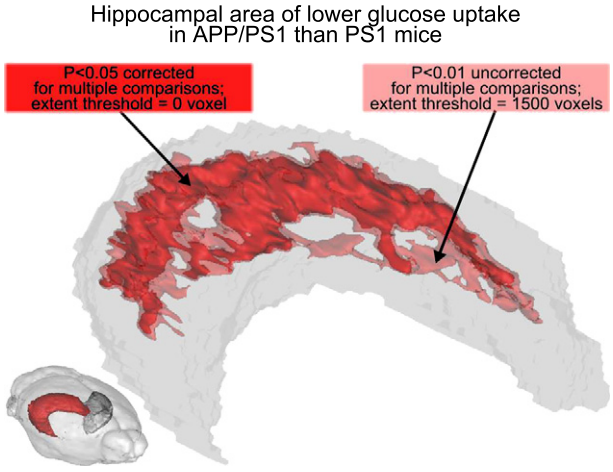

Fig. 8. 3D representation of a cluster displaying hypometabolism in APP/PS1 mice in the hippocampal region obtained without (light red) and with (dark red) correction for multiple comparisons (FDR correction). The restriction of the statistical analysis using a hippocampal mask provided a cluster (~0.74 mm^3) with a metabolic difference between strains equal to ~−22.39%, *i.e.* greater than the difference obtained without correction (~−20.60% measured over ~1.39 mm^3).

The main advantage of our method is that it can quickly provide results without the need to refer to a paper atlas like the one of Paxinos and Franklin (2001). In addition, it requires limited or no expert intervention. To our knowledge, this method, previously used in humans (Tzourio-Mazoyer et al., 2002; Maldjian et al., 2003; Eickhoff et al., 2005; Lehericy et al., 2006), has never yet been applied to autoradiographic data from rodents processed with a voxel-wise approach. Nevertheless, our method remains dependent on the quality and on the number of structures present in the digital atlas. For example, in our study, we were obliged to carry out a manual segmentation of the cingulate and retrosplenial cortexes in the digital atlas in order to study them.

Analysis of metabolic changes detected using the voxel-wise approach guided by a digital atlas

The detection of cluster spreading over several anatomical regions could be due to atlas misregistration or the statistical inferences preset in SPMMouse. To determine the case that corresponds to each cluster concerned, we computed the percentage of cluster voxels that overlapped with atlas-based ROI voxels, as previously performed in human studies (Tzourio-Mazoyer et al., 2002; Eickhoff et al., 2005). Additionally, we measured the activity of subclusters indexed according to the atlas.

Overlap rate between detected clusters and atlas-based segments

The computation of this rate (see Table 3) enabled us to identify clusters entirely contained within a single structure: this was found to be the case in 4 of the 17 clusters detected for the two contrast types. This quantitative method also allowed us to determine which clusters spread over several ROIs, and to calculate the volume of each subcluster assigned to a given atlas-based segment. According to the statistical parameters chosen for our study, we assumed that all subclusters smaller than 0.05 mm^3 were due to atlas misregistration. Similarly, subclusters classified within the ventricles were considered to be due to a registration error. This analysis enabled the automated indexation of 8 of the remaining 13 clusters within various cerebral regions.

Functional analysis of clusters spread over several atlas-based segments

At this stage of the study, 5 clusters were still spread over several anatomical regions. If this was due to the grouping of separate clusters as a consequence of parameters preset in the software, the activity of

subclusters extracted from a "single" cluster would be different. In light of this assumption, the combination of atlas-based and voxel-based approaches permitted us to identify more areas displaying metabolic differences between APP/PS1 and PS1 mice than when we analyzed data using only the voxel-wise approach (see Tables 1 and 4).

The automated splitting of clusters detected by the voxel-wise approach using atlas-based segmentation led to an interesting functional deduction. The hypermetabolism detected in the corpus callosum (white matter not supposed to display activity) in APP/PS1 mice (+27.60% 2-DG uptake when compared to PS1 mice) could have been due to atlas misregistration, as suggested by overlap criteria, or a consequence of the smoothing and normalization steps performed to create the block-face template. Nevertheless, this could also reflect a reduction in the volume of the corpus callosum as highlighted in mouse models of Alzheimer's disease (Redwine et al., 2003; Valla et al., 2006; Lau et al., 2008; Maheswaran et al., 2009b), or a partial volume effect (Valla et al., 2002). Alternatively, this could also reflect a compensation of white matter dysfunction (Desai et al., 2009) or defective communication between the two hemispheres (Vyazovskiy et al., 2008). The hypermetabolism in the olfactory bulb of APP/PS1 mice (+29.37% 2-DG uptake when compared to PS1 mice) shows that this structure has a subcortical part that was not removed, and suggests the involvement of compensatory mechanisms (Wesson et al., 2010). The hyperactivity in the amygdala (+18.03% 2-DG uptake in APP/PS1 mice) could be correlated with previously identified morphological alterations in this structure (Knafo et al., 2009).

All the studies cited above confirm the possible occurrence of hypermetabolism in the corpus callosum, olfactory bulb and amygdala of APP/PS1 mice, on the basis of 2-DG uptake in these animals and in control littermates. The visual identification of detected clusters with the help of a paper atlas, as performed in Dubois et al. (2010), could not have yielded these conclusions. Further investigations focusing on these regions should be carried out to confirm these biological results. However, our work demonstrates the advantages of combining the atlas-based and voxel-based approaches to analyze 3D-reconstructed autoradiographic data: 1) a cluster detected by a voxel-wise approach can be automatically indexed within an anatomical region defined in a digital atlas, and 2) if the cluster spreads over several segments, the atlas can automatically split it into subclusters classified in different ROIs (a task difficult to achieve manually) and subsequent functional analysis can confirm or refine the results obtained.

Small-volume correction using the registered digital atlas

The functional data analyzed in this study involved more than 5.10^6 voxels (image background excluded). The first statistical design tested, taking all voxels into consideration, would have yielded thousands false positives and made it impossible to apply the FDR correction. By using a previously registered atlas-based segmentation to the study-specific template as an explicit mask in the statistical design, we considerably reduced the number of tested voxels (by a factor of 10 to 100). For the contrast type representing APP/PS1 hypometabolism and using a hippocampal mask, we were able to demonstrate differences in metabolism after the application of the FDR correction, at a threshold of significance of 5%. This confirms that the use of a digital atlas to guide the voxel-based approach can refine the results obtained. To our knowledge, this work is the first to successfully achieve small-volume correction in a voxel-wise analysis of autoradiographic data from the rodent brain, using a registered atlas-based segmentation as a mask in the statistical design.

This small-volume correction was successful only when using the hippocampal mask. This could be due to the shape of the ROIs (Frackowiak et al., 2003) or to the percentage of occupancy of the cluster in the region segmented. Indeed, the volume of the hypometabolic subcluster detected in the hippocampus was ≃12% of the volume of the segmented hippocampus. Moreover, this was the only (sub)cluster that occupied more than 10% of the ROI in which it was classified. This seems to mean that the issue of multiple comparisons can be solved using atlas-based segmentation if the cluster is large enough compared to the size of the ROI-mask involved in this step. Additional tests need to be performed using different datasets to define an eventual threshold of efficacy for small-volume correction.

Conclusion

The present study demonstrates that our methodology led to the successful combination of two complementary approaches to the analysis of *post mortem* mouse brain functional images: the MRI-based atlas and the voxel-wise approach. Whereas analysis using an MRI-based atlas is incapable of revealing slight metabolic changes between strains or opposing effects occurring locally within a single structure, the voxel-wise approach requires expert intervention to identify and to localize activated areas and often suffers from the large amount of voxels to be computed in a rodent study. Using an MRI-based 3D digital atlas to steer a voxel-wise analysis thus permitted the prompt indexation of areas of metabolic change at the scale of atlas-based ROIs with limited operator intervention, and a refinement of the statistical results obtained.

This combination of approaches was realized for a study dealing with a small number of unstimulated animals; the number of clusters of activated voxels was not excessive. In the case of a whole brain study comparing groups with greater functional differences, a large number of clusters could be detected by the statistical method. A manual analysis of all of them would thus be very time-consuming and prone to misinterpretation. The application of our combined approach would enable a reduction of the time required for mapping major functional differences between groups of animals and would also be useful in evaluating functional communication between cerebral structures. It would also lead to a lowered risk of errors in the sorting of clusters of voxels according to size or their classification into atlas-based ROIs, as well as according to their probable symmetry into the brain. The potential small-volume correction carried out using the atlas-based segmentation would provide more significant statistical comparisons with a reduced probability of detecting false positives. This is thus a promising approach for the analysis of large *post mortem* and *in vivo* functional datasets, and could find several applications in exploratory studies in the neurosciences. Morphological studies in small animals based on the voxel-wise approach (Lau et al., 2008; Maheswaran et al., 2009a; Sawiak et al., 2009) could for example benefit from the advantages provided by the guidance of voxel-wise analysis using an MRI-based atlas.

Finally, if we were able to accurately determine bregma and lambda (Aggarwal et al., 2009), we could merge all these results and provide supplementary valuable information to biologists used to work with these cranial landmarks.

Acknowledgments

This work was partially supported by the Medicen Paris Région program TransAl. We would like to thank the Sanofi-Aventis Neurodegenerative Disease Group for generously providing the transgenic animals involved in this study.

References

Aggarwal, M., Zhang, J., Miller, M.I., Sidman, R.L., Mori, S., 2009. Magnetic resonance imaging and micro-computed tomography combined atlas of developing and adult mouse brains for stereotaxic surgery. Neuroscience 162 (4), 1339–1350 Sep.

Badea, A., Ali-Sharief, A.A., Johnson, G.A., 2007. Morphometric analysis of the C57BL/6J mouse brain. Neuroimage 37 (3), 683–693 Sep.

Benjamini, Y., Hochberg, Y., 1995. Controlling the false discovery rate: a practical and powerful approach to multiple testing. J. R. Stat. Soc. B 57 (1), 289–300.

Blanchard, V., Moussaoui, S., Czech, C., Touchet, N., Bonici, B., Planche, M., Canton, T., Jedidi, I., Gohin, M., Wirths, O., Bayer, T.A., Langui, D., Duyckaerts, C., Tremp, G., Pradier, L., 2003. Time sequence of maturation of dystrophic neurites associated with abeta deposits in APP/PS1 transgenic mice. Exp. Neurol. 184 (1), 247–263 Nov.

Casteels, C., Vermaelen, P., Nuyts, J., Linden, A.V.D., Baekelandt, V., Mortelmans, L., Bormans, G., Laere, K.V., 2006. Construction and evaluation of multitracer small-animal PET probabilistic atlases for voxel-based functional mapping of the rat brain. J. Nucl. Med. 47 (11), 1858–1866.

Chan, E., Kovacevic, N., Ho, S.K.Y., Henkelman, R.M., Henderson, J.T., 2007. Development of a high resolution three-dimensional surgical atlas of the murine head for strains 129s1/svimj and c57bl/6j using magnetic resonance imaging and micro-computed tomography. Neuroscience 144 (2), 604–615 Jan.

Collins, D.L., Neelin, P., Peters, T.M., Evans, A.C., 1994. Automatic 3D intersubject registration of MR volumetric data in standardized Talairach space. J. Comput. Assist. Tomogr. 18 (2), 192–205.

Delatour, B., Guégan, M., Volk, A., Dhenain, M., 2006. *In vivo* MRI and histological evaluation of brain atrophy in APP/PS1 transgenic mice. Neurobiol. Aging 27 (6), 835–847 Jun.

Deriche, R., 1987. Using Canny's Criteria to Derive a Recursively Implemented Optimal Edge Detector. Internal Journal of Computer Vision 1 (2), 167–187 Mai.

Desai, M.K., Sudol, K.L., Janelsins, M.C., Mastrangelo, M.A., Frazer, M.E., Bowers, W.J., 2009. Triple-transgenic Alzheimer's disease mice exhibit region-specific abnormalities in brain myelination patterns prior to appearance of amyloid and tau pathology. Glia 57 (1), 54–65 Jan.

Dice, L.R., 1945. Measures of the amount of ecologic association between species. Ecology 26 (3), 297–302 Jul.

Dorr, A.E., Lerch, J.P., Spring, S., Kabani, N., Henkelman, R.M., 2008. High resolution three-dimensional brain atlas using an average magnetic resonance image of 40 adult C57Bl/6J mice. Neuroimage 42 (1), 60–69 Aug.

Dubois, A., Hérard, A.-S., Flandin, G., Duchesnay, E., Besret, L., Frouin, V., Hantraye, P., Bonvento, G., Delzescaux, T., 2008. Quantitative validation of voxel-wise statistical analyses of autoradiographic rat brain volumes: application to unilateral visual stimulation. Neuroimage 40 (2), 482–494 Apr.

Dubois, A., Hérard, A.-S., Delatour, B., Hantraye, P., Bonvento, G., Dhenain, M., Delzescaux, T., 2010. Detection of significant changes in regional cerebral glucose uptake in APP/PS1 mouse model of Alzheimer's disease using voxel-wise statistical analysis. Neuroimage 51 (2), 586–598 Jun.

Eickhoff, S.B., Stephan, K.E., Mohlberg, H., Grefkes, C., Fink, G.R., Amunts, K., Zilles, K., 2005. A new spm toolbox for combining probabilistic cytoarchitectonic maps and functional imaging data. Neuroimage 25 (4), 1325–1335 May.

Eickhoff, S.B., Heim, S., Zilles, K., Amunts, K., 2006. Testing anatomically specified hypotheses in functional imaging using cytoarchitectonic maps. Neuroimage 32 (2), 570–582 Aug.

Frackowiak, R., Friston, K., Frith, C., Dolan, R., Price, C., Zeki, S., Ashburner, J., Penny, W., 2003. Human Brain Function, 2nd Edition. Academic Press.

Friston, K.J., Frith, C.D., Liddle, P.F., Frackowiak, R.S., 1991. Comparing functional PET images: the assessment of significant change. J. Cereb. Blood Flow Metab. 11 (4), 690–699.

Friston, K.J., Holmes, A.P., Poline, J.B., Grasby, P.J., Williams, S.C., Frackowiak, R.S., Turner, R., 1995. Analysis of fMRI time-series revisited. Neuroimage 2 (1), 45–53.

Genovese, C.R., Lazar, N.A., Nichols, T., 2002. Thresholding of statistical maps in functional neuroimaging using the false discovery rate. Neuroimage 15 (4), 870–878 Apr.

Hérard, A.S., Dubois, A., Escartin, C., Tanaka, K., Delzescaux, T., Hantraye, P., Bonvento, G., 2005. Decreased metabolic response to visual stimulation in the superior colliculus of mice lacking the glial glutamate transporter GLT-1. Eur. J. Neurosci. 22 (d), 1807–1811.

Hess, A., Lohmann, K., Gundelfinger, E., Scheich, H., 1998. A new method for reliable and efficient reconstruction of 3-dimensional images from autoradiographs of brain sections. J. Neurosci. Methods 84 (1–2), 77–86.

Johnson, G.A., Ali-Sharief, A., Badea, A., Brandenburg, J., Cofer, G., Fubara, B., Gewalt, S., Hedlund, L.W., Upchurch, L., 2007. High-throughput morphologic phenotyping of the mouse brain with magnetic resonance histology. Neuroimage 37 (1), 82–89 Aug.

Knafo, S., Venero, C., Merino-Serrais, P., Fernaud-Espinosa, I., Gonzalez-Soriano, J., Ferrer, I., Santpere, G., DeFelipe, J., 2009. Morphological alterations to neurons of the amygdala and impaired fear conditioning in a transgenic mouse model of Alzheimer's disease. J. Pathol. 219 (1), 41–51 Sep.

Lancaster, J.L., Woldorff, M.G., Parsons, L.M., Liotti, M., Freitas, C.S., Rainey, L., Kochunov, P.V., Nickerson, D., Mikiten, S.A., Fox, P.T., 2000. Automated Talairach atlas labels for functional brain mapping. Hum. Brain Mapp. 10 (3), 120–131 Jul.

Lau, J.C., Lerch, J.P., Sled, J.G., Henkelman, R.M., Evans, A.C., Bedell, B.J., 2008. Longitudinal neuroanatomical changes determined by deformation-based morphometry in a mouse model of Alzheimer's disease. Neuroimage 42 (1), 19–27 Aug.

Lebenberg, J., Hérard, A.-S., Dubois, A., Dauguet, J., Frouin, V., Dhenain, M., Hantraye, P., Delzescaux, T., 2010. Validation of MRI-based 3D digital atlas registration with histological and autoradiographic volumes: an anatomofunctional transgenic mouse brain imaging study. Neuroimage 51 (3), 1037–1046 Jul.

Lee, J., Ahn, S.-H., Lee, D., Oh, S., Kim, C., Jeong, J., Park, K., Chung, J.-K., Lee, M., 2005. Voxel-based statistical analysis of cerebral glucose metabolism in the rat cortical deafness model by 3D reconstruction of brain from autoradiographic images. Eur. J. Nucl. Med. Mol. Imaging 32 (6), 696–701.

Lehericy, S., Bardinet, E., Tremblay, L., de Moortele, P.-F.V., Pochon, J.-B., Dormont, D., Kim, D.-S., Yelnik, J., Ugurbil, K., 2006. Motor control in basal ganglia circuits using fMRI and brain atlas approaches. Cereb. Cortex 16 (2), 149–161 Feb.

Maheswaran, S., Barjat, H., Bate, S.T., Aljabar, P., Hill, D.L.G., Tilling, L., Upton, N., James, M.F., Hajnal, J.V., Rueckert, D., 2009a. Analysis of serial magnetic resonance images of mouse brains using image registration. Neuroimage 44 (3), 692–700 Feb.

Maheswaran, S., Barjat, H., Rueckert, D., Bate, S.T., Howlett, D.R., Tilling, L., Smart, S.C., Pohlmann, A., Richardson, J.C., Hartkens, T., Hill, D.L.G., Upton, N., Hajnal, J.V., James, M.F., 2009b. Longitudinal regional brain volume changes quantified in normal aging and Alzheimer's APP/PS1 mice using MRI. Brain Res. 1270, 19–32 May.

Malandain, G., Bardinet, E., Nelissen, K., Vanduffel, W., 2004. Fusion of autoradiographs with an MR volume using 2-D and 3-D linear transformations. Neuroimage 23 (1), 111–127.

Maldjian, J.A., Laurienti, P.J., Kraft, R.A., Burdette, J.H., 2003. An automated method for neuroanatomic and cytoarchitectonic atlas-based interrogation of fMRI data sets. Neuroimage 19 (3), 1233–1239 Jul.

Mattes, D., Haynor, D., Vesselle, H., Lewellen, T., Eubank, W., 2003. PET-CT image registration in the chest using free-form deformations. IEEE Trans. Med. Imaging 22.

Mevel, K., Desgranges, B., Baron, J.-C., Landeau, B., la Sayette, V.D., Viader, F., Eustache, F., Chtelat, G., 2007. Detecting hippocampal hypometabolism in mild cognitive impairment using automatic voxel-based approaches. Neuroimage 37 (1), 18–25 Aug.

Morrow, T.J., Paulson, P.E., Danneman, P.J., Casey, K.L., 1998. Regional changes in forebrain activation during the early and late phase of formalin nociception: analysis using cerebral blood flow in the rat. Pain 75 (2–3), 355–365 Apr.

Nguyen, P., Holschneider, D., Maarek, J., Yang, J., Mandelkern, M., 2004. Statistical parametric mapping applied to an autoradiographic study of cerebral activation during treadmill walking in rats. Neuroimage 23 (1), 252–259.

Paulson, P.E., Wiley, J.W., Morrow, T.J., 2007. Concurrent activation of the somatosensory forebrain and deactivation of periaqueductal gray associated with diabetes-induced neuropathic pain. Exp. Neurol. 208 (2), 305–313 Dec.

Paxinos, G., Franklin, K., 2001. The Mouse Brain in Stereotaxic Coordinates. Academic Press, San Diego, CL.

Poldrack, R.A., 2007. Region of interest analysis for fMRI. Soc. Cogn. Affect. Neurosci. 2 (1), 67–70 Mar.

Prima, S., Ourselin, S., Ayache, N., 2002. Computation of the mid-sagittal plane in 3D brain images. IEEE Trans. Med. Imaging 21 (2), 122–138.

Redwine, J.M., Kosofsky, B., Jacobs, R.E., Games, D., Reilly, J.F., Morrison, J.H., Young, W.G., Bloom, F.E., 2003. Dentate gyrus volume is reduced before onset of plaque formation in pdapp mice: a magnetic resonance microscopy and stereologic analysis. Proc. Natl. Acad. Sci. U. S. A. 100 (3), 1381–1386 Feb.

Rueckert, D., Sonoda, L.I., Hayes, C., Hill, D.L., Leach, M.O., Hawkes, D.J., 1999. Nonrigid registration using free-form deformations: application to breast MR images. IEEE Trans. Med. Imaging 18 (8), 712–721.

Sadowski, M., Pankiewicz, J., Scholtzova, H., Ji, Y., Quartermain, D., Jensen, C.H., Duff, K., Nixon, R.A., Gruen, R.J., Wisniewski, T., 2004. Amyloid-beta deposition is associated with decreased hippocampal glucose metabolism and spatial memory impairment in APP/PS1 mice. J. Neuropathol. Exp. Neurol. 63 (5), 418–428 May.

Sawiak, S.J., Wood, N.I., Williams, G.B., Morton, A.J., Carpenter, T.A., 2009. Voxel-based morphometry in the R6/2 transgenic mouse reveals differences between genotypes not seen with manual 2D morphometry. Neurobiol. Dis. 33 (1), 20–27 Jan.

Schweinhardt, P., Fransson, P., Olson, L., Spenger, C., Andersson, J.L.R., 2003. A template for spatial normalisation of MR images of the rat brain. J. Neurosci. Methods 129 (2), 105–113.

Sharief, A.A., Johnson, G.A., 2006. Enhanced t2 contrast for MR histology of the mouse brain. Magn. Reson. Med. 56 (4), 717–725 Oct.

Sharief, A.A., Badea, A., Dale, A.M., Johnson, G.A., 2008. Automated segmentation of the actively stained mouse brain using multi-spectral MR microscopy. Neuroimage 39 (1), 136–145 Jan.

Swanson, L., 1998. Brain Maps: Structure of the Rat Brain, 2nd Revised Edition. Elsevier Science, Amsterdam.

Talairach, J., Tournoux, P., 1988. Co-planar stereotaxic atlas of the human brain: 3-dimensional proportional system: an approach to cerebral imaging. Thieme Medical Publishers. January.

Tzourio-Mazoyer, N., Landeau, B., Papathanassiou, D., Crivello, F., Etard, O., Delcroix, N., Mazoyer, B., Joliot, M., 2002. Automated anatomical labeling of activations in SPM using a macroscopic anatomical parcellation of the MNI MRI single-subject brain. Neuroimage 15 (1), 273–289 Jan.

Valla, J., Chen, K., Berndt, J.D., Gonzalez-Lima, F., Cherry, S.R., Games, D., Reiman, E.M., 2002. Effects of image resolution on autoradiographic measurements of posterior cingulate activity in pdapp mice: implications for functional brain imaging studies of transgenic mouse models of Alzheimer's disease. Neuroimage 16 (1), 1–6 May.

Valla, J., Schneider, L., Reiman, E.M., 2006. Age- and transgene-related changes in regional cerebral metabolism in PSAPP mice. Brain Res. 1116 (1), 194–200 Oct.

Vyazovskiy, V.V., Cirelli, C., Tononi, G., Tobler, I., 2008. Cortical metabolic rates as measured by 2-deoxyglucose-uptake are increased after waking and decreased after sleep in mice. Brain Res. Bull. 75 (5), 591–597 Mar.

Wesson, D.W., Levy, E., Nixon, R.A., Wilson, D.A., 2010. Olfactory dysfunction correlates with amyloid-beta burden in an Alzheimer's disease mouse model. J. Neurosci. 30 (2), 505–514 Jan.

Zijdenbos, A.P., Dawant, B.M., Margolin, R.A., Palmer, A.C., 1994. Morphometric analysis of white matter lesions in MR images: method and validation. IEEE Trans. Med. Imaging 13 (4), 716–724.